Journal of Power Sources 309 (2016) 99–107

Contents lists available at ScienceDirect

Journal of Power Sources

journal homepage: www.elsevier.com/locate/jpowsour

On-demand supply of slurry fuels to a porous anode of a direct carbon fuel cell: Attempts to increase fuel-anode contact and realize long-term operation

Chengguo Li, Hakgyu Yi, Donggeun Lee*

School of Mechanical Engineering, RIMT, Pusan National University, Busandaehak-ro 63beon-gil, Geumjeong-gu, Busan 46241, Republic of Korea

HIGHLIGHTS

- A potentially continuous fuel supply with increasing fuel-anode contacts in a DCFC.
- Of importance was the size match between the anode pores and fuel particles.
- Maximal power density under the optimal size-matching reached 645 mW cm^{-2}.
- More than 20-h steady operation was achieved at a current density of 700 mA cm^{-2}.

ARTICLE INFO

Article history:
Received 16 October 2015
Received in revised form
18 January 2016
Accepted 21 January 2016
Available online xxx

Keywords:
Direct carbon fuel cell (DCFC)
Triple-phase boundary
Porous anode
Continuous fuel supply

ABSTRACT

In this paper, we propose a novel idea that might allow resolution of the two biggest challenges that hinder practical use of direct carbon fuel cells (DCFC). This work involved 1) the use of three types of porous Ni anode with different pore sizes, 2) size matching between the anode pores and solid fuel particles in a molten-carbonate (MC) slurry, and 3) provision of a continuous supply of fuel-MC slurry through the porous Ni anode. As a result, larger numbers of smaller pores in the anode were preferred for extending the triple phase boundary (TPB), as long as the fuel particles were sufficiently small to have full access to the inner pore spaces of the anode. For example, the maximal power density achieved in the case of optimal size matching, reached 645 mW cm^{-2}, which is 14-times greater than that for the case of poorest size-matching and 64-times larger than that for a non-porous anode, and lasted for more than 20 h. After 20 h of steady operation at a fixed current density (700 mA cm^{-2}), the electric potential slightly decreased due to partial consumption of the fuel. The cell performance readily recovered after restarting the supply of MC-fuel slurry.

1. Introduction

Recently, a large number of studies have been performed on direct carbon-fuel-cells (DCFC) because of their great potential for use in applications affecting energy and environment. The highest theoretical efficiency (near 100%) [1–7], does not require CO_2 separation from flue gas in a conventional power plant [1,2], and the usable fuels are diverse: any carbon-containing fuel, including coal, biomass, and even organic waste [7–11]. These potential advantages have undoubtedly led to the recent attention attracted by DCFC.

Because DCFC systems use solid rather than gaseous fuels (e.g., H_2, CO, and CH_4), two big issues are raised. One relates to the unacceptably low activity of the fuel electrode, caused mainly by very limited formation of triple phase boundaries[1] (TPBs) between solid

[1] The concept of triple phase boundary could be drawn from an anodic reaction in Eq (1) (will be shown). To produce electrons, the fuel (C) should have a chance to encounter the carbonate ions (CO_3^{2-}). As the ions transported from a cathode could be available only in the liquid-phase MC, the fuel particles should be in contact with the MC. In addition, as-produced electrons need to be drawn from the anode and then delivered to the cathode in order to continue the cathodic reaction (Eq (2)). This requires additional contact between the electrode and the site of anodic reaction. Thus, effective electrochemical reaction presumably occurs only at coincident contacting sites between three different phases: solid fuel particles, a liquid electrolyte, and a solid electrode. This is why TPB formation is limited when using solid fuels that are hard to handle, compared to gaseous fuels.

* Corresponding author.
E-mail address: donglee@pusan.ac.kr (D. Lee).

http://dx.doi.org/10.1016/j.jpowsour.2016.01.080
0378-7753/

fuel, anode, and electrolyte [12–14]. The second relates to their too short operation time owing to discontinuous refueling [1,15–17]. As for the issue of the limited TPBs, there are a few previous reports proposing new ideas to overcome this problem. In some of the studies on DCFC systems based on SOFC, for example, metal/metal oxide powders were mixed with solid electrolyte powder to form cermet-type anodes (e.g., Ni-YSZ and Ni SDC). The pores in the anode could be used as extended surfaces when being filled with carbon, leading to an increase in the TPBs [12,14]. Li et al. [13] used thermal decomposition of methane at temperatures above 800 °C to produce carbon inside a porous cermet. Despite large increases in the TPBs (expected) and its high working temperature (700–900 °C), both of which could accelerate the electrochemical reaction kinetics, the power density was barely 110 mW cm^{-2}, still far from the levels required.

More recently, we attempted to maximize the TPB by filling the pores of porous Ni foam with carbon powder, together with a ceria coating of Ni foam to enhance the electrolyte (molten carbonate, MC) wettability of the Ni. A button cell of MC-based DCFC having a C-filled Ni anode was tested, and the result showed that the power density of the button cell was increased by a factor of seven, as compared to a flat interface between fuel and electrode [18]. However, the button cell structure of the DCFC limits long-term cell operation due to the impracticality of refueling the porous anode. Most recently, we changed our direction by producing the carbon fuels inside the porous anode, rather than supplying solid fuels from outside. Thermal decomposition of gaseous hydrocarbons was quite successful for this purpose, and this approach allowed for control of the morphology and amount of fuel along with great enhancement of the TPBs [19]. We found that a material with a 1-D structure (carbon nanofibers) was preferred for filling the pore space of the anode, and was successful at raising the power density to ~500 mW cm^{-2}. Thus, we believe that the idea of using porous Ni foam was quite successful.

As for the issue of discontinuous refueling, Cooper et al. [16] presented another design allowing for continuous fuel supply in the form of a MC-C slurry into the cell. This resulted in a peak power density of 55 mW cm^{-2} at 800 °C, and the longest operation of the cell was for 30 h. LLNL [17] designed a self-feeding cell with an inclined electrode that could be refueled pneumatically. The design concept was extended for a 75–150 W, 5-cell self-feeding bipolar stack (120–160 mW cm^{-2} per cell). Heydron et al. [20] proposed another DCFC-concept based on a supply of carbon powder through a fluidized-bed-type assembly. Their fuel supply system offers advantages such as continuous fueling with easy scale up, and simple separation of heavier ash components from carbon. Though they successfully demonstrated continuous fuel feeding, the physical contact between carbon particles floating in the gas and the anode was very limited. Overall, there has been no success in resolving both of the issues simultaneously: maximizing TPBs with continuous fuel feeding.

Here, we propose a novel solution to both challenges. This involves four types of Ni anode with different pore sizes, and the continuous feeding of graphite powder-MC slurry into the Ni anode. We attempted to maximize the TPBs by optimizing the size match between the fuel particles and the anode pores. As a result, the size of the anode pores needed to be as small as possible, as long as the fuel powder was small enough to get inside them. Measurements of I–V, at the optimal size combination, demonstrated that the current fuel-feeding anode has produced a power density of ~645 mW cm^{-2} for 20 h. After partial consumption of the fuel powder, the power generation readily recovered after restarting the supply of fuel-MC slurry through the anode.

2. Experimental

Fig. 1 shows a schematic of the three-electrode electrochemical cell that was developed in this study, based on the design of Vutetakis [4]. A 6-cm long, 1.8-cm thick, cylindrical piece of porous Ni foam was used as an anode (WE), after being spot-welded to a flat-plate-type silver current collector (6 cm high × 0.4 cm thick). Four types of Ni foam with different pore sizes (20, 40, 60, 80 ppi) were considered. The counter electrode (CE) and reference electrode (RE) were made from a silver sheet (surface area 3.2 cm^2) spot-welded to a silver wire. The silver parts were each sheathed in a 12-mm diameter closed-bottom alumina tube. A 1.0-mm hole at the bottom of the alumina sheath allowed carbonate ions to conduct between the electrodes through the MC electrolyte.

We considered two types of graphite powder with two different particle sizes (average diameter 0.15 and 1.3 mm). The specific surface area, pore size, and volume of the fuel particles were measured by a gas sorptometer (Autosorb-1, Quantachrome) using nitrogen adsorption at 77 K and Brunauer–Emmett–Teller (BET) analysis. The results are summarized in Table 1. Both of the fuel particles have similar BET properties and their specific surface areas both remain in the non-porous levels. Thus, we did not pay attention to the surface area of the fuels.

Scanning electron microscopy (SEM; S-4800, Hitach, 15 kV) equipped with energy dispersive spectrometer (EDS) was used to explore the microstructure of the porous Ni anode. Fig. 2 shows SEM images of three-dimensional (3D) porous structures of the four types of Ni anodes used in this study. EDS measurement for the anodes confirmed that there are no foreign species (but Ni) beyond detectable lower limit. X-ray Diffraction (XRD, D/MAX-2400, Rigaku) was also conducted to analyze the purity of the Ni anodes by scanning the angle of 2θ in the range of 10–90° at a rate of 6° min^{-1} while irradiating Cu Kα X-ray (30 kV, 40 mA, 0.15218 nm). In Fig. S1, the 2θ positions of the three major peaks are 44.4, 51.7, and 76.3°, all of which are very close to the JCPDS data (44.5, 51.8, and 76.4°, respectively) for pure metallic Ni. This suggests that the Ni anode was very likely metallic Ni without any further crystalline contaminants. A similar result was also shown in our previous publication [18].

To make the MC-carbon slurry, 350 g of dry carbonate powder (consisting of 32-wt% Li_2CO_3 and 68-wt% K_2CO_3) was mixed with 50 g of graphite powder of two different particle sizes in an alumina container, and then heated at 700 °C to melt the carbonates. As shown in Fig. 1, an alumina stirring-rod was placed in the center of the container and rotated to stir the slurry. This served to trap some of the fuel particles inside the porous WE. The amount of fuel powder trapped inside was gradually increased with stirring time. If the internal pore space of the WE were completely filled with fuel powder, further rotation of the slurry would not cause any difference in electricity production. We tested several stirring periods and confirmed that 10 min of stirring was long enough for complete fueling of the WE. Thus, the stirring continued for only 10 min, and then was stopped to perform electrochemical measurements. Though this intermittent stirring was employed to measure the timing and duration of fuel consumption, steady fuel feeding is possible, in principle, by stirring continuously.

Prior to measurement of electrochemical performance, any residual oxygen in the system was removed by flowing CO_2 gas at a rate of 50 ml min^{-1} to the CE and RE, during the warm-up process of the system. When the operating temperature of 700 °C was attained, a mixture of CO_2 and O_2 (mole ratio of 2:1) was injected into the CE and the RE at a total flow rate of 100 ml min^{-1}. During the electrochemical reaction of carbon, Ar gas was continually supplied to the WE at 200 ml min^{-1} in order to purge the CO_2 gas produced.

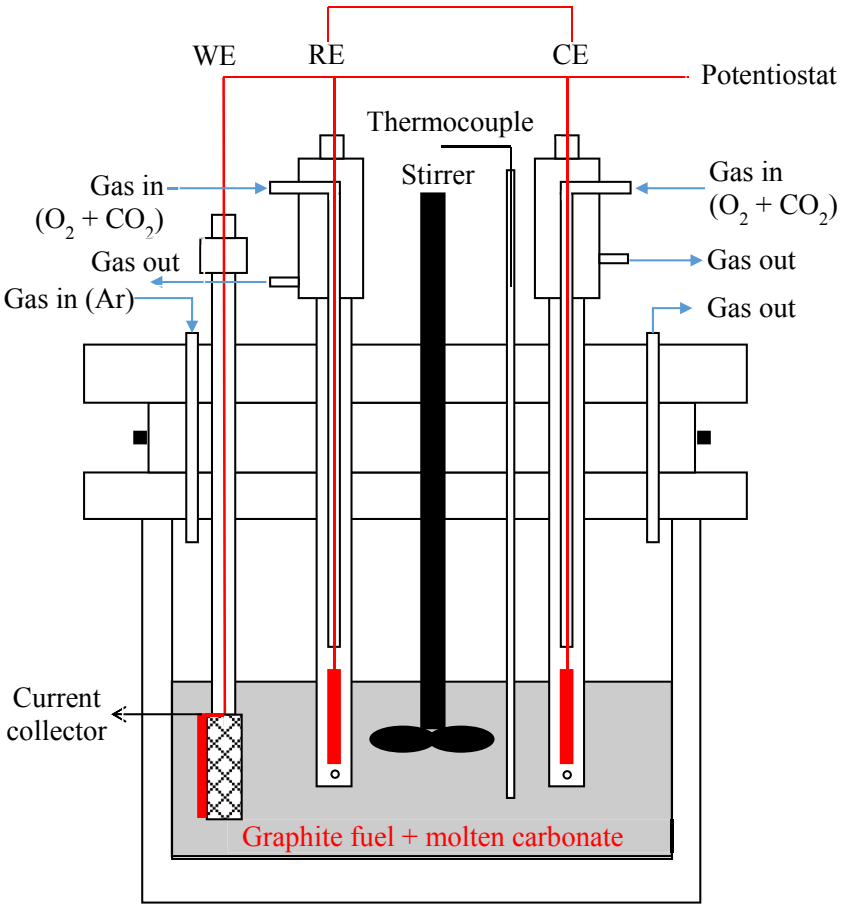

Fig. 1. Schematic diagram of the 3-electrode MC-based DCFC system.

Table 1
BET results for two types of graphite particles with average diameters of 1.3 and 0.15 mm.

Fuel powder diameter (mm)	N_2 adsorption at 77 K		
	S_{BET} ($m^2\ g^{-1}$)	V_{total} ($cm^3\ g^{-1}$)	D_{pore} (nm)
1.3	1.00	0.0043	16.6
0.15	0.84	0.0038	17.4

When the graphite-fueled WE is immersed in the MC, contacts between the fuel particles and the Ni networks of the WE are believed to play a role in the TPBs. Hence, the fuel particles undergo the following anodic reaction inside the porous WE:

$$C + 2CO_3^{2-} \rightarrow 3CO_2 + 4e^- \quad (1)$$

This equation indicates a direct route for complete electrochemical oxidation of carbon. In the CE (cathode), the provided gas mixtures are believed to react electrochemically with incoming electrons by Eq. (2).

$$O_2 + 2CO_2 + 4e^- \rightarrow 2CO_3^{2-} \quad (2)$$

The anodic and cathodic reactions constitute the overall reaction in Eq. (3), indicating that the only product gas (CO_2) is emitted from the anode, which eliminates the need for CO_2 separation from flue gas of fuel-burning power plants.

$$C + O_2 \rightarrow CO_2 \quad (3)$$

The electric current-potential characteristics of the present DCFC system were measured using a SP-150 Potentiostat/Galvanostat analyzer (Neoscience, Korea) with a scan rate of 1 mV s^{-1}. Because the RE, being in the proximity of the WE, is electrically separated from the CE, potential change of the WE could be monitored independently of changes that may occur at the CE [4,6,11]. Hence, the electric potential (V) in this study indicates the voltage difference between the WE and RE, while the electric current between the WE and CE was monitored. Under the open-circuit condition, the potential of the RE was confirmed to be very close to that of the CE, and the electric potential (vs. RE) was regarded as the open circuit voltage (OCV).

It should also be noted that the outer surface area (33.9 cm^2) of the cylindrical anode (WE) was used as the reference surface area for estimating the power and current density. The power density (P) was obtained by multiplying the current density (I: the current divided by the outer surface area of the anode) by the electric potential. In order to understand the I–V characteristics better, electrochemical impedance spectroscopy (EIS) was measured with the SP-150 analyzer over the frequencies from 0.2 Hz to 40 kHz.

3. Results and discussion

3.1. Size matching issue of fuel powder and the pores in Ni anodes

Fig. 2(a)-(d) exhibit clear decreases in pore size and wire thickness of the Ni anodes when increasing the porosity from 20 to 80 ppi. The pores of the Ni anodes are mostly composed of hexagonal meshes; however, the largest pores of the 20-ppi Ni anode

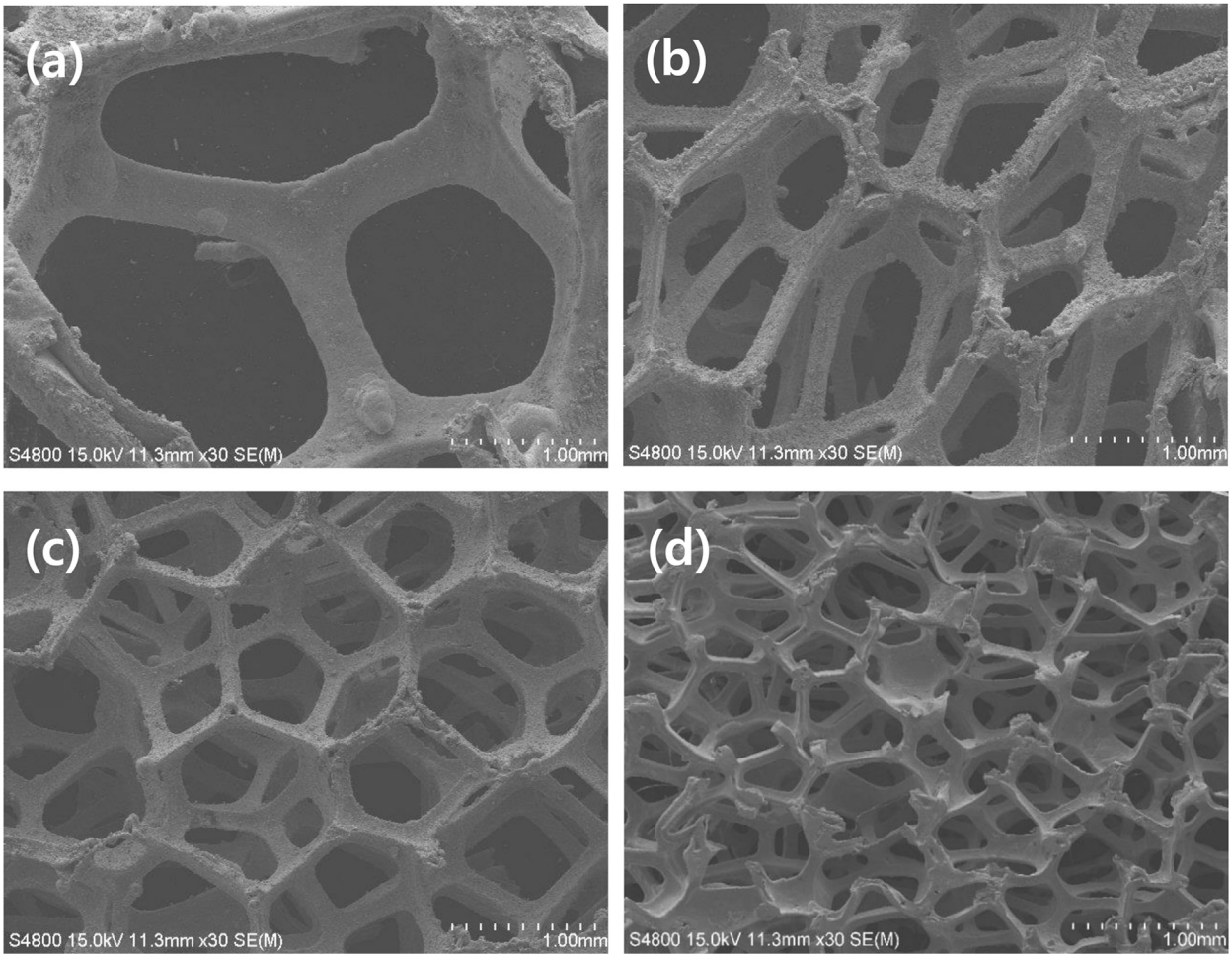

Fig. 2. SEM images of porous Ni anodes with four different pore sizes: a) 20-ppi, b) 40-ppi, c) 60-ppi, and d) 80-ppi.

tend to be compressed, in contrast to isotopic hexagonal pores in the 80-ppi Ni anode. For such anisotropic pores, an average value of the largest and shortest lengths of the pores was used for sizing the pore. This kind of SEM image analysis was repeated for more than 100 pores in each kind of Ni anode, and pore size distributions were obtained for the four types of Ni anodes.

Fig. 3 shows that the pore size of the 20-ppi Ni anode was distributed from 0.6 to 2.2 mm, with a mode size of ~1.4 mm (see solid line with open circles). A line with solid triangles or solid squares (Fig. 3) represents the particle-size distribution of the fine or coarse graphite powder. It was observed that coarse graphite powder had a size distribution similar to that of the pores of the 20-ppi Ni anode, so the powder could get inside the 20-ppi anode. However, the coarse powder appeared too large to get into the 40, 60, and 80-ppi Ni anodes. For example, a small fraction of the powder (<1.1 mm) could enter the large pores of the 40-ppi anode. In the case of the 60-ppi anode, only a minor fraction of the powder (<0.9 mm) could have had limited access to the inside of the anode. Finally, the coarse powder is not likely to have had access to the inside of the 80-ppi anode. Regarding the triple phase boundary, the 20-ppi anode was expected to make the best combination with the coarse graphite powder.

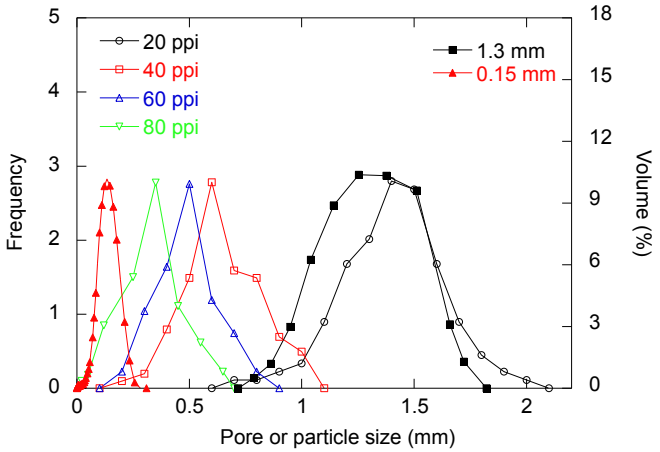

Fig. 3. Size distributions of graphite particles and pores of the four types of anodes.

To study further the fuel particle-pore size matching issue, we considered much smaller (fine) graphite powder (0.02–0.25 mm) with average diameter of 0.15 mm (see Fig. 3). The use of the fine fuel powder allowed the graphite fuel to have full access to the inside pore spaces of all anodes tested in this study. Under these circumstances, any change in the porosity of the anode (in terms of ppi number) could alter not only the size of the pore space caged with Ni wires, but also the total number (as well as the entire length) of the Ni wires in different anodes with the same apparent volume. When a porous anode containing the fine graphite powder is immersed in a pool of MC, any contacts between the powder and

Ni wires could serve as TPBs. As a result, the 80-ppi anode, which has the smallest pores and the largest number of Ni wires inside, is anticipated to provide the maximum number of contacts with the fine fuel powder and thus show the best electrochemical performance.

To verify these conjectures about size-matching, I–V and I–P characteristics were measured for the first matched group: coarse graphite powder of 1.3 mm vs. 20, 40, 60, and 80-ppi Ni anodes. The porous anodes were all cylindrical with a constant outer surface area. A solid (nonporous) Ni cylinder with the same surface area was also tested as a reference anode with minimal surface contact with the fuels. When applying the coarse graphite powder for the non-porous Ni cylinder at 700 °C, the I–P results (see Fig. S2) indicate a very small power density of 11.5 mW cm^{-2} at a current density of 40 mA cm^{-2}. Such low power is attributed to insufficient formation of the TPBs, which made this anode the least active. Upon use of the 20-ppi anode, in which the coarse fuel powder had the best internal contact among the anodes, the maximal power density dramatically increased (250 mW cm^{-2}) along with a 10-time increase in current density, as shown in Fig. 4(a). When the anode was more porous (from 40 to 80 ppi), the maximal power density and current density both clearly decreased. This observation is exactly consistent with the aforementioned view of the fuel particle-pore size paradigm. Note that the maximal power density of this 80-ppi anode was 46 mW cm^{-2}, still much higher than that of the non-porous anode. In addition to the fact that the coarse fuel powder could have (albeit limited) access to the surface vicinity of the 80-ppi anode (Fig. 3), the surface roughened by the Ni wires presumably helps to trap more fuel particles, compared to the smooth surface of the non-porous anode, leading to considerable increase in TPBs.

To highlight this positive prospect, the fine fuel powder (as small as 0.15 mm) was tested for the four types of anode (the second matched group). Fig. 4(b) demonstrates clearly that the size matching, in relation to TPB formations, is critical. The maximal power density increased with ppi of the anodes, from 315 to 645 mW cm^{-2}. The highest power density for the 80-ppi anode was almost 64 times larger than that of the non-porous anode. At the same time, the maximum current density was >2500 mA cm^{-2}, comparable to the typical capacity of a H_2-fueled MCFC. It is worth noting that the open circuit voltage (OCV) in the case of the fine fuel powder was ~1.0 V, relatively large compared with ~0.8 V for the coarse powder. This increase in the OCV appears consistent with the observation noted by Nabae et al. [21] that, for their hybrid button-cell SO-DCFC system fueled with MC and carbon powder, the OCV increased with increasing carbon content. This was in response to the improved contact between the carbon and the anode plate, although their power density remained low (~12 mW cm^{-2}).

To examine the possible role of the fuel-anode contact or TPB on cell performance, EIS measurements were performed at 700 °C for all the combinations shown in Fig. 4(a) and (b): coarse or fine graphite powders vs. each of the four types of anodes plus a non-porous anode. Fig. 5(a) clearly shows that the EIS profiles for the coarse fuel powder could be altered very significantly by the degree of size matching, depending on the anode pore size. The EIS curves were fitted using equivalent circuit models with series and parallel combinations of solution resistance, charge transfer resistance, and Warburg element. As a result, the solution resistance indicated by the left x-intercept of hemi-circles was found to be almost invariant (~0.08 Ω cm^2) regardless of the pore size of the anodes. As indicated by the size of the hemi-circles, the charge transfer resistance (R_{ct}) clearly decreased with better matching between fuel-particle size and pore size (from 80 to 20 ppi): 0.62, 0.52, 0.41, and 0.27 Ω cm^2, for the 80, 60, 40, and 20-ppi anodes, respectively. These are all an order of magnitude smaller than that of the nonporous Ni anode (~4.8 Ω cm^2). Because the R_{ct} is regarded as a measure of the kinetics of electrochemical reactions [22], the fact that the R_{ct} of the 80-ppi anode was larger than that of the 20-ppi anode might indicate limited access of the coarse fuel particles to the 80-ppi anode. Moreover, it was not surprising to confirm that the highest power density was observed at the lowest R_{ct} for the 20-ppi anode, when using coarse graphite powder (see Fig. 4a).

In Fig. 5(b), the fine graphite powder (0.15 mm diameter) exhibited further decrease of the R_{ct} with increasing ppi number of the anode: R_{ct} values were 0.26, 0.2, 0.1, and 0.05 Ω cm^2, for the 20, 40, 60, and 80-ppi anodes, respectively. Because the fine powder had full access to the pore space of all the anodes we considered, higher ppi numbers or smaller anode pores with more Ni wires (see Fig. 2) would provide more surfaces for the fuel powder. Recalling the peak power density and R_{ct} values of each case (Figs. 4b and 5b), one may notice again that the R_{ct} values of the anodes (inversely proportional to the power density), seem to be closely related to the degree of size matching, or with contacts between fuel and anode. It was thus of particular interest to investigate quantitatively the relations between the number of contacts and R_{ct}, as well as the maximum power density.

It is impossible to estimate the real number of fuel-anode contacts, without knowledge of the true surface area of the Ni wires, as well as the packing state of the fuel particles inside the anodes.

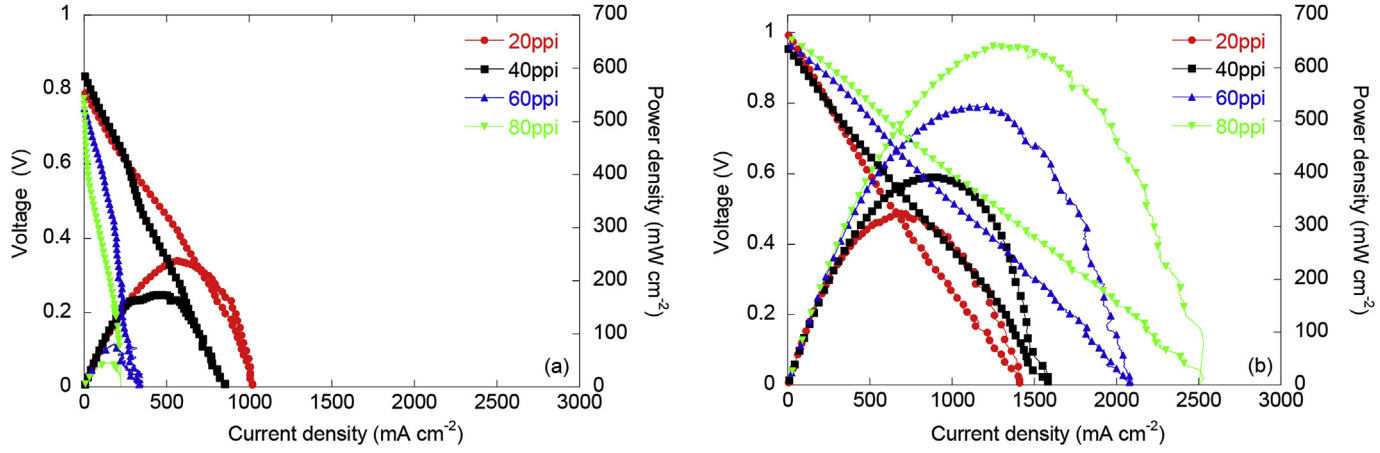

Fig. 4. I-V characteristics of the DCFC system employing four types of anodes fueled with graphite particles of two different average diameters: a) 1.3 mm and b) 0.15 mm.

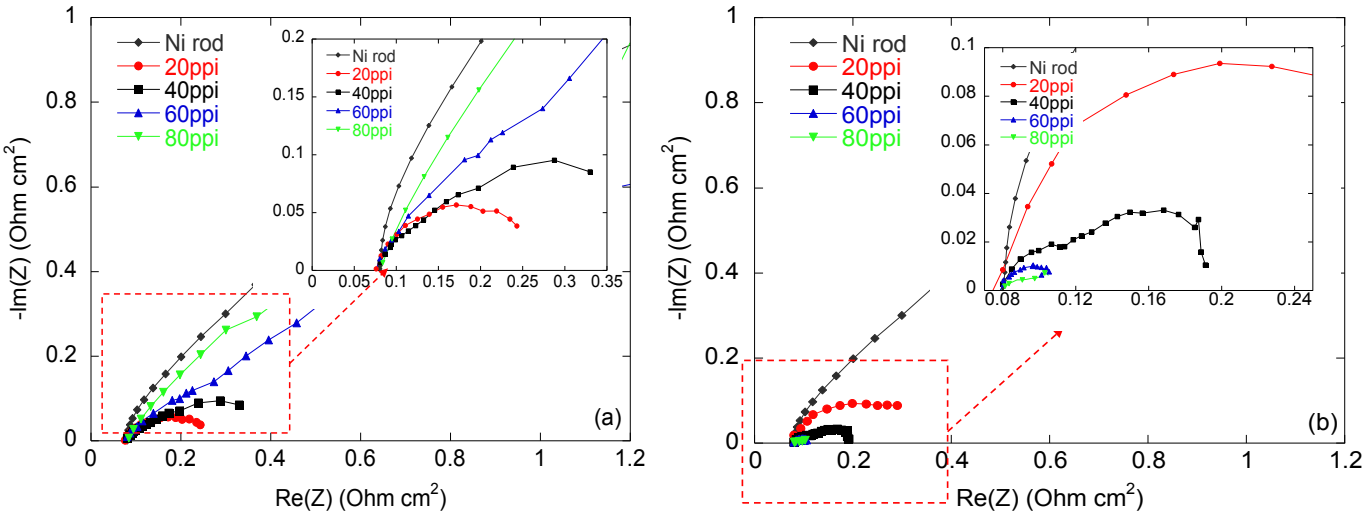

Fig. 5. Electrochemical impedance spectra of the DCFC systems with four types of anode (20-ppi, 40-ppi, 60-ppi, and 80-ppi) fueled with two different sizes of fuel particles: a) 1.3 mm and b) 0.15 mm; for comparison, a non-porous Ni cylinder of the same shape as the anodes was tested; the dotted rectangular region was magnified and shown with inset.

Alternatively, we considered an upper limit of the contact number between the fuel and porous anode. The assumptions were a case of perfect contact, and that same-sized spherical fuel particles were closely packed and lined up on the entire surface of the anode wires. This would be the best situation we could imagine, provided that the fuel particles were sufficiently small. Based on this, the maximum contact numbers were estimated as follows. Recall that the original porous anode was shaped like a cylinder with similar radius and length. The mass of the blank (unfueled) Ni anode was measured and then divided by the bulk density (8.9 g cm^{-3}) of Ni to yield the net volume of the anode. The average cross-section area of Ni wires was obtained from the wire thickness measured from Fig. 2; then the net volume was divided by the cross-section area to estimate the entire length of Ni wires in the anode. Given the average diameter of the fuel particles, calculation of the maximum contact number was straightforward. Table 2 summarizes all of the data used for the calculation.

Not surprisingly, Fig. 6(a) shows that R_{ct} is in linear inverse proportion to the maximum number of fuel-anode contacts for the four anodes with fine graphite powder. Under the size-matching condition, the anode with the higher ppi numbers very likely provides more active sites along with more elongated Ni wires. Unlike the case of fine fuel powder, only small fractions of the coarse powder overlap in size with the pores of the 40, 60 and 80-ppi anodes, so that only 5, 3, and 1% (respectively) of the powder is in internal contact with the anodes, and participates in the anodic reaction. Thus, the maximum contact number for the coarse fuel particles with the other three anodes (40–80 ppi) in Table 2 should be further corrected by multiplying by the fraction, so as to consider this size mismatch. This is why the contact number (corrected) of the coarse powder decreases with increasing the ppi number in Fig. 6(a), showing a steeper linear profile. Overall, such different contact states depend on the degree of particle-pore size matching, and are summarized schematically in the inset: red solid lines of different lengths signify longer Ni wires available in a higher-ppi anode. The large and small spheres represent coarse and fine powder particles lined up. Only one or two large spheres are depicted sitting on the longer wire for the 40 and 80-ppi anodes, in order to represent their limited access due to the size mismatch.

In Fig. 6(b), all of the maximum power densities found from Fig. 4(a) and (b) are presented against the corresponding R_{ct} values from Fig. 5(a) and (b). It is interesting to see that all of the data lay closely on a single curved line showing a steady decline, regardless of the degree of size matching. An equation resulting from the third-degree polynomial fitting was added in Fig. 6(b), in an attempt to provide a quantitative correlation as a sort of guidance. This suggests that the effect of size mismatch is reflected mainly by an increase of the R_{ct}, and that the R_{ct} is in turn, the most significant factor determining power generation. It is noted again that the R_{ct} was reduced by an order of magnitude simply by best matching the sizes.

Despite these promising results, there is a concern as to the reaction pathway of the fuels. Other workers [23,24] reported that there is another (indirect) route of carbon electro-oxidation: the MC could react with carbon to form CO (see Eqs. (4) and (5)), and the CO could be used as an auxiliary (gaseous) fuel to produce electricity (Eq. (6)).

Table 2
Calculation of the maximum (uncorrected) contact number between fuel particles and the Ni networks of the anodes.

Anode types	Average diameter of Ni wires (mm)	Entire length of Ni wires (m)	Average diameter of fuel particles (mm)	Max. contact number[a] (×1000)
20-ppi	0.62	0.93	1.3	0.76
			0.15	6.20
40-ppi	0.18	11.91	1.3	9.16
			0.15	79.4
60-ppi	0.15	21.61	1.3	16.2
			0.15	144.06
80-ppi	0.15	36.86	1.3	28.3
			0.15	245.6

[a] The maximum contact numbers are uncorrected values for the size mismatch.

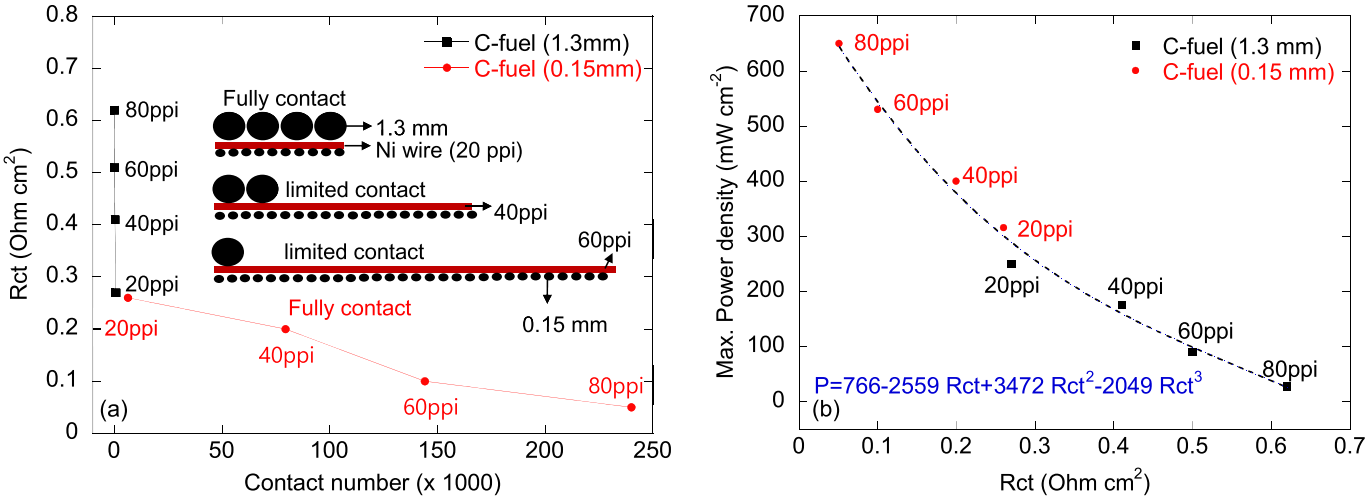

Fig. 6. Correlations between a) maximum (corrected) fuel-anode contact number and the charge transfer resistance of R_{ct}, b) R_{ct} and maximum power density; the dotted line and the equation represent the result of third degree polynomial fitting.

$$C + M_2CO_3 \rightarrow M_2O + 2CO \quad (4)$$

$$C + M_2O \rightarrow 2M + CO \quad (5)$$

where M is Li or K.

$$CO + CO_3^{2-} \rightarrow 2CO_2 + 2e^- \quad (6)$$

If this indirect route is significant in the present system, the chemical reactions of Eqs. (4) and (5) should occur at the OCV condition (in which Eq. (6) is not allowed). This implies that the only product gas (CO) in Eqs. (4) and (5) should be detected from the off gas from the anode under the OCV condition ($I = 0$ mA cm^{-2}). To check this possibility, we measured the anode-emitting gas composition (CO vs. CO_2) under two different conditions ($I = 0$ vs. 700 mA cm^{-2}), using gas chromatography (8610C, SRI instrument). As shown in Fig. S3, we could not see any distinct CO signal under the OCV condition. At that time, a minor level of CO_2 was detected within 0.2 vol%, which could have originated from the fuel itself. At 700 mA cm^{-2}, the exhaust gas was almost pure CO_2 with negligible levels of CO. Both results suggest that the carbon fuels very likely follow the direct route and that increase in the solid fuel-anode contacts causes an order-of-magnitude enhancement in the current and power generation.

3.2. Long-term operation of the DCFC with easy refueling

As mentioned in the Introduction, DCFC technology has not yet reached a stage to address long-term durability of the system, or even long-term operation, mainly because of the impracticality of refueling with fuel powders. Because solid fuels are difficult to handle, a refueling concept that involves the use of a fuel powder-MC slurry might be a convenient option. When the fuel-feed ended after 10 min of stirring in the system shown in Fig. 1, the measurement of electric potential began and continued for 20 h at a fixed electric current. For example, considering the I–V curves of the coarse graphite powder in Fig. 5(a), 0.6 V was chosen as an initial potential for the four types of anodes. The corresponding value of current density was 87 mA cm^{-2} for the 60-ppi anode (used even for the 80-ppi anode), and 260 mA cm^{-2} for both the 40-ppi and 20-ppi anodes. The designated current density was fixed for the next long-term operation of the cell.

Fig. 7(a) shows the result of 20 h of operation of the four anodes containing the coarse graphite powder. When there was a size mismatch (e.g., the 40, 60, and 80-ppi anodes), the electric potential dropped rapidly from the initial voltage to 0.5, 0.4, and 0.28 V in the first 30 min, and then showed a stepwise voltage decrease to 0.21, 0.18, and 0.12 V in 135, 60, and 36 min, respectively, for the anodes. In contrast, the 20-ppi anode showed no voltage drop for 20 h. The rapid voltage drops, observed only in the cases of size mismatch, likely support the conjecture that only roughened surface sites are available for use by the coarse fuel particles, because the anode pores were too small to admit them. The particles were rapidly consumed and lost contact with the anode surface, leading to a large decrease in the amount of fuel in the TPB. Thus, the short lifetimes (2, 1, and 0.6 h) of the 40, 60, and 80 ppi anodes, are believed to reflect the amount of carbon fuels trapped in the anodes.

As for the fine graphite powder (0.15 mm), the electric voltages were monitored over time at a fixed current density of 700 mA cm^{-2} for all the anodes. Fig. 7(b) shows very promising results for long-term operation of the DCFC. The four porous anodes, regardless of their pore sizes (as long as the pores were larger than the fuel particles), appeared to preserve the extended TPBs longer and thereby prevent a visible drop in voltage. Among the anodes in this case, the 20-ppi anode (Fig. 7b) was found to be the least active and less durable: this anode supported the lowest voltage (~0.45 V) for 10 h from the beginning, and then showed a slight voltage decrease. For the 40-ppi anode, a little higher voltage of 0.6 V was maintained for 15 h, and then began to decrease. The performance improvement was even more pronounced when using the more porous anodes (60 and 80 ppi), leading to higher voltages, and with no voltage loss during the entire test period (20 h).

To test the potential for facile (or continuous) fuel supply in the present system, the I–V curve for the 20-ppi anode containing the fine fuel powder, was measured before and after the long-term operation experiment (20 h at 700 °C; see Fig. 7b). The 20-ppi anode, the worst case with the fine powder, was selected to visualize the system potential for easy refueling. Fig. 8shows that all performance indexes decreased after 20 h of operation, in response to partial fuel consumption in the WE: the OCV declined from 1.0 to 0.83 V, and the maximum power density dropped from 325 to 238 mW cm^{-2}. Next, the fuel-MC slurry, still in the cell container

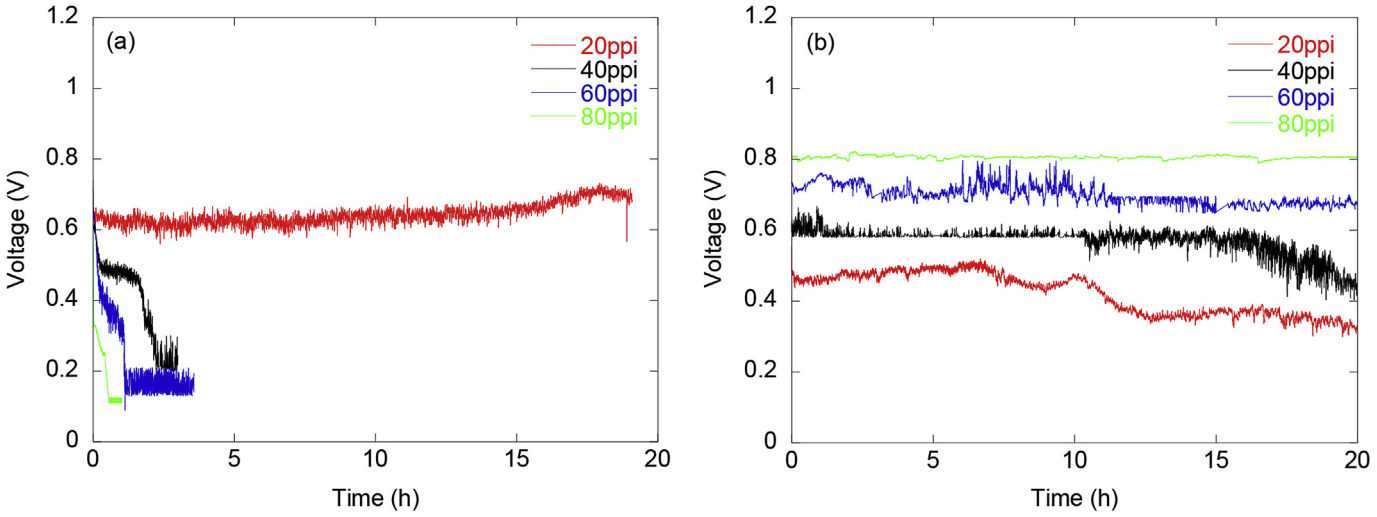

Fig. 7. Lifetime test results for the four types of anodes, each used with the two types of fuel particles: a) 1.3 mm and b) 0.15 mm.

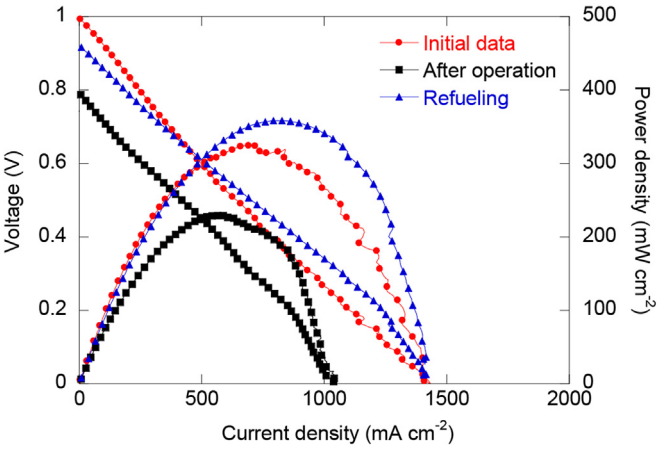

Fig. 8. Refueling test for the 20-ppi anode combined with 0.15-mm fine fuel particles performed at 700 oC: Cell performance was measured twice at the beginning and after 20 h of operation, to assure partial fuel consumption. After 10 min of refueling, the test was repeated.

(see Fig. 1), was rotated for another 10 min to replace the fuel consumed. Fig. 8 shows again that the 10-min fuel replenishment was quite successful. The system recovered its initial performance in terms of power and current density, and the OCV. Though this is not a true demonstration of a continuous fuel supply, we did at least realize an intermittent supply of fuel on demand, which clearly helps maximize fuel utilization. To the best of our knowledge, this is the first demonstration of a (potentially) continuous supply of fuel in the form of fuel-MC slurry, while maximizing the triple phase boundary.

4. Conclusions

In this paper, a novel idea was proposed with the aim of resolving the two most critical issues that hinder commercialization of DCFC: limited formation of triple phase boundary and discontinuous fuel supply. The key was to provide a fuel-MC slurry to a porous anode with optimized fuel-particle size with respect to the pore size of the anode. This approach could offer two unique functions of the anode. One is that the porous anode woven with long Ni wires could provide extended active surfaces for the fuel particles, leading to a large increase in the contact between fuel and anode, an order-of-magnitude decrease in the charge transfer resistance, and thereby maximizing the anode performance. The other is to realize a continuous, or at least an intermittent, on-demand supply of as much fuel as needed; this could maximize the fuel utilization. This idea was demonstrated by employing four types of porous Ni anodes with different pore sizes, each paired with coarse and fine graphite powder. When the fuel particles were sufficiently small to have full access to the internal pore spaces: under the size-matching condition, the anode with the smallest pores showed the maximum power density of 645 mW cm^{-2}; the maximum current density of 2500 mA cm^{-2}; the longest lifetime (>20 h) with no apparent voltage drop. In contrast, when the fuel particle size was mismatched with the pore size, the contact between fuel and anode was very limited, causing serious performance degradation. After 20 h of steady operation of the size-matched system at a fixed current of 700 mA cm^{-2}, the system performance that had degraded by as much as 33% was found to recover readily by stirring the slurry fuel. Impedance spectra revealed that the maximum power density was linearly correlated with the charge-transfer resistance, and that this was significantly influenced by the degree of fuel-anode contact, or triple phase boundary.

Acknowledgements

This work was supported by the Global Frontier R&D Program of the Center for Multiscale Energy Systems funded by the National Research Foundation under the Ministry of Education, Science and Technology, Korea (No. 2012M3A6A7054863), and also by the research on “Development of the Preparation Technology of 0.1–10 μm Sized Metal Powders and Fine-Components for Micro Electronics” of MKE (Ministry of Knowledge Economy) and ISTK (Korea Research Council for Industrial Science and Technology of Republic of Korea.

Appendix A. Supplementary data

Supplementary data related to this article can be found at http://dx.doi.org/10.1016/j.jpowsour.2016.01.080

References

[1] S. Giddey, S.P.S. Badwal, A. Kulkarni, C. Munnings, Prog. Energ. Combust. 38 (2012) 360–399.
[2] D. Cao, Y. Sun, G. Wang, J. Power Sources 167 (2007) 250.
[3] A. Elleuch, A. Boussetta, K. Halouani, J. Electroanal. Chem. 668 (2012) 99–106.
[4] D.G. Vutetakis, D.R. Skidmore, H.J. Byker, J. Electrochem. Soc. 34 (1987) 3027–3035.
[5] X. Li, Z. Zhu, R.D. Marco, J. Bradley, A. Dicks, Energy Fuels 23 (2009) 3721–3731.
[6] X. Li, Z.H. Zhu, R.D. Marco, A. Dicks, J. Bradley, S. Liu, G.Q. Lu, Ind. Eng. Chem. Res. 47 (2008) 9670–9677.
[7] X. Li, Z. Zhu, R.D. Marco, J. Bradley, A. Dicks, J. Power Sources 195 (2010) 4051–4058.
[8] M. Dudek, P. Tomczyk, R. Socha, M. Hamaguchi, Int. J. Hydrogen Energy 39 (2014) 12386–12394.
[9] C. Lee, W. Kim, Int. J. Hydrogen Energy 40 (2015) 5475–5481.
[10] N. Kaklidis, I. Garagounis, V. Kyriakou, V. Besikiotis, A. Arenillas, J.A. Menendez, G.E. Marnellos, M. Konsolakis, Int. J. Hydrogen Energy 40 (2015) 14353–14363.
[11] S. Ahn, S. Eom, Y. Rhie, Y. Sung, C. Moon, G. Choi, D. Kim, Energy 51 (2013) 447–456.
[12] J. Yu, B. Yu, Y. Li, Int. J. Hydrogen Energy 38 (2013) 16615–16622.
[13] C. Li, Y. Shi, N. Cai, J. Power Sources 196 (2011) 4588–4593.
[14] X. Xu, W. Zhou, F. Liang, Z. Zhu, Appl. Energy 108 (2013) 4022–4029.
[15] A. Kulkarni, F.T. Ciacchi, S. Giddey, C. Munnings, S.P.S. Badwal, J.A. Kimpton, D. Fini, Int. J. Hydrogen Energy 37 (2012) 19092–19102.
[16] J.F. Cooper, R.L. Krueger, N.J. Cherepy, US Pat., 0017380 A1, 2003.
[17] J.F. Cooper, N.J. Cherepy, R.L. Krueger, U. S. Pat., 6878479, 2005.
[18] C. Li, E.K. Lee, Y.T. Kim, D. Lee, Int. J. Hydrogen Energy 39 (2014) 17314–17321.
[19] C. Li, H. Yi, T. Jalalabadi, D. Lee, J. Power Sources 294 (2015) 284–291.
[20] B. Heydron, S. Crouch-Baker, New York, IOP publishing, 2006.
[21] Y. Nabae, K.D. Pointon, T.S. Irvine, Energy Environ. Sci. 1 (2008) 148–155.
[22] B.C. Tubilla, C. Xu, J.W. Zondlo, K. Sabolsky, E.M. Sabolsky, J. Power Sources 238 (2013) 227–235.
[23] W. Hirotatsu, F. Tomoaki, O. Ken, J. Power Sources 273 (2015) 340–350.
[24] J.W. Kim, H.G. Lee, Metall. Mater. Trans. B 32B (2001) 17–24.